39 Ma U-Pb ZIRCON AGE FOR THE SHAKI-RASH GABBRO IN THE BULFAT IGNEOUS COMPLEX, KURDISTAN REGION, IRAQI ZAGROS SUTURE ZONE: RIFTING OF AN INTRA-NEOTETHYS CENOZOIC ARC

Sarmad Asi Ali ✉

Department of Applied Geology, Kirkuk University, Iraq, and GeoQuEST Research Centre, University of Wollongong, Australia.

✉ *Corresponding author, email: sarmad@uow.edu.au*

ABSTRACT

The suprasubduction Bulfat Igneous Complex in NE Iraq is one of the discontinuous Neotethys oceanic lithosphere fragments preserved in the Zagros region. Reported here are new geochronological, petrological and geochemical data from this assemblage. At the study locality, Eocene arc-related magmatic rocks are intruded by extensive dykes of Shaki-Rash gabbro. The key reason to focus on these rocks is the remarkable lack of hydrothermal alteration, including preservation of very fresh olivine. Besides olivine the gabbros contain plagioclase and clinopyroxene, with lesser orthopyroxene, biotite, brown hornblende and alkali feldspar. From mineral chemistry, the crystallization conditions of the olivine gabbros are ~ 950-1050°C and ~ 5-3 kbar. Shaki-Rash gabbro shows alkaline affinity. SHRIMP U-Pb dating of magmatic zircon from the gabbro yielded a mean $^{206}Pb/^{238}U$ age of 39.0±0.5 Ma (Eocene). Most of the Shaki-Rash gabbro samples have Ti/V of 100 to 50 and fall in the back-arc basin (BAB) and alkaline fields, while on a Nb/Yb-Th/Yb diagram, most samples fall within the MORB-OIB array and plot in proximity to E-MORB. Primitive-mantle-normalized trace-element patterns show enrichment in the large ion lithophile elements without depletion of the high-field-strength elements. These geochemical signatures and their field setting advocate for the formation of these dikes in an extensional tectonic environment, such as an intra-arc rift.

INTRODUCTION

Intra-oceanic arcs are the simplest kind of subduction systems because the over-riding plate consists of oceanic rocks, contrasting with the inherent complexity of arcs built on continental margins. Nonetheless, there are huge variations in the physical characteristics of intra-oceanic arcs, especially in terms of convergence rate, life span, roughness and thickness of sediment cover on the subducting slab (Larter and Leat, 2003). Intra-oceanic arcs erupt magmas with diverse compositions that reflect their position above the subduction zone, ranging from boninitic to alkaline (Kimura and Stern, 2008). Stress fields can vary on a short timeframe in geodynamically complex convergent margins, leading to the onset of arc-rifting transition with an associated change in magma compositions (e.g., Pearce et al., 2005). Such scenarios have been well-documented in the southwestern Pacific (Taylor and Karner, 1983; Hawkins et al., 1984; Gill and Whelan, 1989; Pearce et al., 2005; Kimura and Stern, 2008). In this paper I present the first evidence for rifting of an Eocene arc in the Iraqi sector of the Zagros collision zone. This is shown by zircon U-Pb dating (using SHRIMP) and the petrogenesis of gabbroic rocks emplaced late in the Bulfat Igneous Complex in the Iraqi Zagros Suture Zone. Implications for closure of the Neotethys ocean are discussed.

GEOLOGICAL FRAMEWORK

The Bulfat Igneous Complex (100 km² extent in Iraq) is one of the discontinuous oceanic lithosphere fragments found in the Zagros region and outcrops at Jabal Bulfat, 30 km east of Qala Deza City, NE Iraq (Jassim et al., 2006;

Aswad et al., 2011; Ali et al., 2012; 2013; 2016; Fig. 1). The Bulfat Igneous Complex is part of the ophiolite-bearing Upper Allochthon Gimo-Qandil Group, which is composed of lithic (metavolcanic) sedimentary rocks of Late Cretaceous (Albian-Cenomanian) age (Jassim et al., 2006). The Upper Allochthon Gimo-Qandil Group was thrust over the Cenozoic Lower Allochthon (Walash-Naopurdan Groups) which, in turn, overlies radiolarian cherts (Qulqula Formation) and platform carbonates (Balambo Formation) of the Mesopotamian Proto-foreland. On the basis of recent studies (Aswad et al., 2011; Aziz et al., 2011; Ali et al., 2012; 2013; 2016), these two allochthonous sheets were juxtaposed and amalgamated into a single nappe (Walash-Penjween Subzone) following the closure of the Neotethys. The Upper Allochthon Gimo-Qandil Group (originally named the Bulfat Group by Jassim et al., 1982) was intruded by voluminous gabbro-diorite intrusions, plus late stage differentiates of syenite and nepheline syenite, forming epizonal multiphase intrusive bodies during an early Cenozoic (Paleocene-Eocene) magmatic episode (Jassim et al., 2006; Aswad et al., 2013; Fig. 2).

The Bulfat Igneous Complex comprises a series of ultramafic, olivine gabbro, hornblende gabbro and diorite intrusions along with minor syenite and granite. Aswad et al. (2013) concluded that the Wadi Rashid plutonic rocks of the Bulfat Igneous Complex at Qala Deza were emplaced into the Albian-Cenomanian ophiolite-bearing Gimo-Qandil Group terrane during the Paleogene (45 Ma, K-Ar dating). They form composite intrusions with an arc affinity (Aswad et al., 2013). These Paleogene rocks and their Cretaceous hosts are tectonically separated from the structurally underlying thrust slice of the coeval Walash-Naopurdan arc-backarc complex (Eocene-Oligocene) found in the same general area (Ali et al., 2013). In addition, Aswad et al.
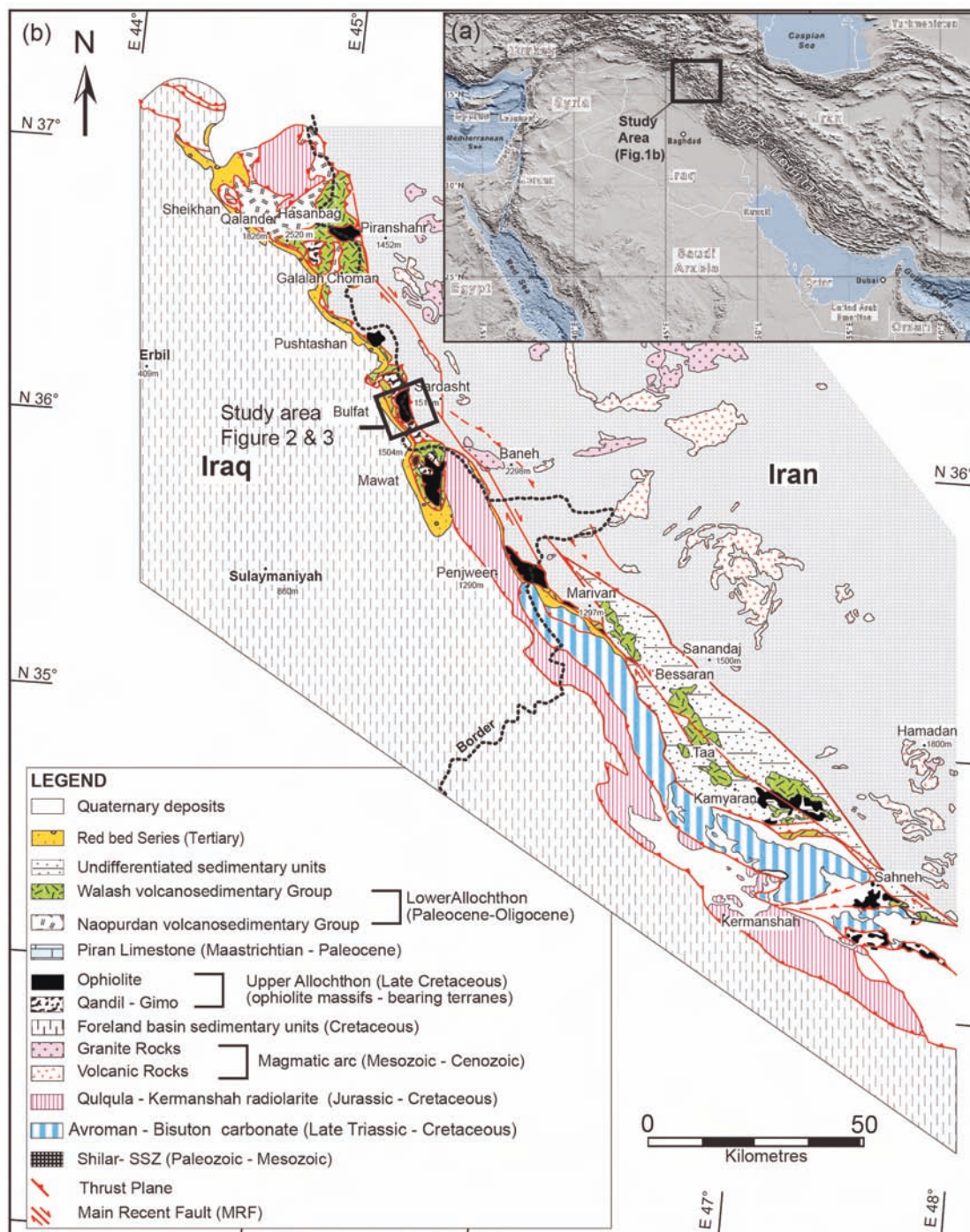
Fig. 1 - (a) Location of the study areas within the Zagros Suture Zone (after Ali et al., 2012); (b) Geological map of the Zagros suture zone along the Iraq-Iran border, showing the location and tectonic division of the study areas (after Ali et al., 2013).

(2016) presented a model for the closure of the Iraq section of Neotethys, involving subduction starting in the Cretaceous, and lasting ≥ 60 million years, with final closure of the ocean involving double subduction systems in the Eocene.

Aswad et al., (2016) determined ^{40}Ar/^{39}Ar ages for the Bulfat Igneous Complex: 39.23±0.21 Ma on igneous hornblende from the gabbro and 38.87±0.24 Ma on biotite from an associated granite. Consequently the complex appears to be significantly younger and is thus unrelated to the host Albian-Cenomanian Gimo-Qandil Group suprasubduction assemblage. The main ~ 39 Ma pluton was intruded by smaller bodies of olivine gabbro, which are the focus of this study (see Fig. 4f).

FIELD OCCURRENCE AND SAMPLING STRATEGY

The exact shapes and sizes of the intrusive complexes are unknown because they stretch into Iran, from where no data is presently available. The Iraqi section is about 15-19 km in a NNW-SSE direction and up to 5-7 km in width. The complex is tilted towards the East (Buda, 1993). Contact metamorphosed calcareous skarn rocks occur on mountain tops (above 2300 m) and most probably represent the roof of the intrusive body. The exposed thickness of the complex is about 1500 m (Buda, 1993). The lower part of the complex comprises tectonically emplaced peridotites. In the middle there are gabbro-diorites and in the upper part there are more alkaline rocks (e.g., nepheline syenite which occurs
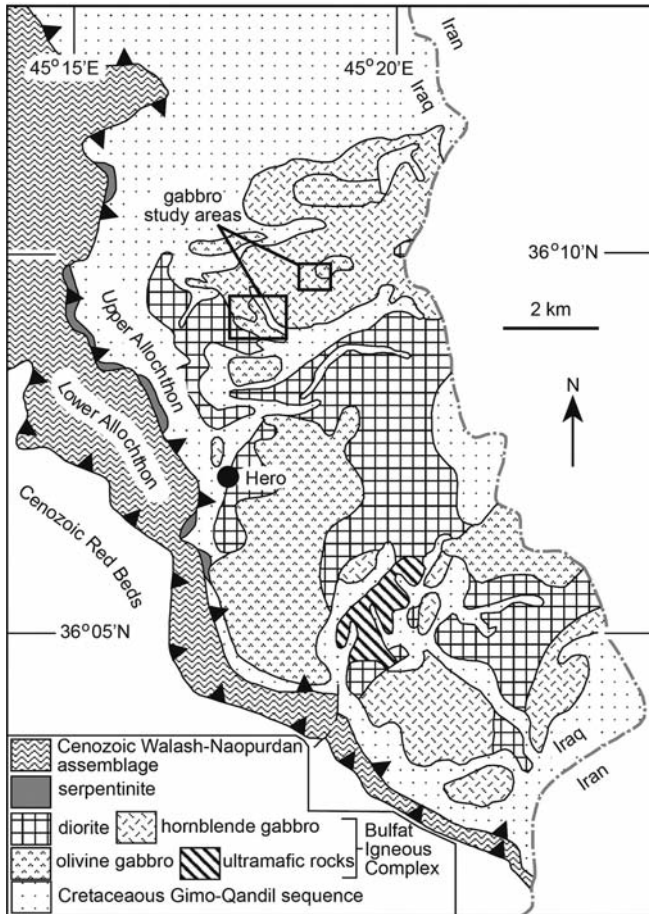
Fig. 2 - Geological Map of Bulfat Igneous Complex, Qala Deza, NE Iraq (after Aswad et al., 2016).

olivine gabbros in the Iraqi suprasubduction assemblages. The gabbroic rocks of this study were collected from the Shaki-Rash Mountain located between longitudes 45°17'11"E and 45°17'46"E and latitudes 36°08'59.6"N and 36°09'38.6"N about 30 km east of Qala Deza City, NE Iraq (Figs 2 and 3). They were emplaced into much larger Cenozoic gabbroic intrusions of the Bulfat Igneous Complex that exhibit wide contact aureoles against host Late Cretaceous arc rocks. Field evidence shows that these younger Shaki-Rash gabbroic rocks appear as swarms of dykes that are up to 50 cm wide and can be followed laterally for hundreds of metres with chilled margins of only a few centimetres. Unlike parts of the older host intrusions, foliated varieties are uncommon. In addition calc-schist xenoliths are very rare in the Shaki-Rash gabbro which demonstrates that these younger intrusions are less contaminated than the older phase of the mafic Bulfat Igneous Complex.

ANALYTICAL TECHNIQUES

Microprobe mineral analysis

Mineral chemistry was determined using a Scanning Electron Microscopy (SEM) utilizing Energy Dispersive Spectrometry (EDS). Analyses were undertaken at the Electron Microscopy Centre facilities (EMC, Wollongong University, Australia) on a JEOL JSM-6490LA SEM with an SDD EDS detector, using Oxford Instruments AZtec suite from an Oxford X-maxN 80mm² SDD. The SEM was run at a low vacuum (so that coating was not necessary) with an accelerating voltage of 15 kV and a beam current of ~ 5 nA. Analyses were performed using 1024 channels with 10 eV per channel, with an automated counting time (until enough counts are collected in the spectrum for quantification). The analytical accuracy of anhydrous phases such as feldspar is 0.1-0.2 wt%.

SHRIMP U-Pb analytical method and data appraisal

Due to artificial hazards in the field area, several small samples were collected on a one day excursion. After consumption of material for thin section making and whole

just below the contact with the calcareous skarn rocks).

This study presents mineralogical, petrological and geochemical data from Shaki-Rash gabbroic rocks to the northeast of Hero town, NE Iraq. The mineral chemistry data represent the first detailed mineralogical analyses of fresh

Fig. 3 - Satellite image over the Bulfat Igneous Complex shows the location of the samples.

rock geochemistry, small portions of several Shaki-Rash gabbro was combined to make a composite sample for zircon separation. Even so, the total weight of sample used for this was < 200 g. This of course is not an ideal situation, given that the yield of zircons from gabbros would already be generally low, because they only rarely crystallize from zircon-saturated pockets of late residual melt.

Heavy minerals were concentrated using heavy liquid

Fig. 4 - Photomicrographs (a-e) of Shaki-Rash gabbro rocks viewed with crossed nicols: (a) Intergranular texture which the angular interstices between plagioclase grains are occupied by grains of ferromagnesian minerals such as olivine, biotite and iron-titanium oxides, sample SR17; (b) Poikilitic texture, with subhedral equant olivine crystals enclosed in a single large plagioclase crystal, sample SR9; (c) Igneous kaersutite in olivine gabbro, sample SR16; (d) Ilmenite as irregular interstitial grains or inclusions in olivine and kaersutite, with Ti-magnetite along the cleavages and cracks of olivine and/or surrounded by biotite and olivine, sample SR9; (e) Orthopyroxene rim at olivine-plagioclase interface, sample SRga2; (f) field photograph showing a dyke of Shaki-Rash gabbro, intruding older gabbro. OL- olivine; Pl- plagioclase; Opx- orthopyroxene; Kf- alkali-feldspar; Krs- kaersutite; Bio- biotite; IO- iron oxide (after Kretz, 1983).

and isodynamic separation techniques at the mineral separation laboratory of the Research School of Earth Sciences, Australian National University (ANU). Using a binocular microscope, the > 3.3 specific gravity concentrate was hand-picked, and only one ca. 200 μm zircon, grain was found. The single recovered grain was cast into an epoxy resin disc along with reference Temora zircons (Black et al., 2003). After the epoxy cured, the mount was ground to a mid-section level through the grains and then polished. Cathodoluminescence (CL) imaging was used to document the grains.

U-Th-Pb analyses of the zircons were undertaken on the ANU SHRIMP RG instrument following analytical protocols of Williams (1998), with the raw data being reduced using ANU softwares 'PRAWN' and 'Lead'. The beam size employed was ~ 25 μm with an O_2^- primary beam current of ~ 4 nA. Measurements of $^{206}Pb/^{238}U$ from the unknown zircon grain were calibrated using the Temora reference material (U-Pb ages concordant at 417 Ma; Black et al., 2003). The reference zircon SL13 (U = 238 ppm) located in a set-up mount was used to calibrate U and Th abundance in the unknown zircon. The ISOPLOT program (Ludwig, 2003) was used to assess and plot the reduced and calibrated data. The results are plotted in a Tera-Wasserburg Concordia diagram prior to correction for common Pb. The reason for plotting them without correction for common Pb is to demonstrate that given the small amount of common Pb in these zircons, the data already have close to concordant U-Pb ages, prior to correction. Weighted mean $^{206}Pb/^{238}U$ ages were calculated both prior to correction for common Pb, and after correction using the measured ^{204}Pb and the Cumming and Richards (1975) Pb composition for the likely age of the zircon.

Major-element and trace-element analyses

Whole-rock major- and trace-element X-ray fluorescence (XRF) analyses were carried out with a Spectro-Analytical Instrument (XEPOS) energy-dispersive spectrometer fitted with a Si-diode detector at the School of Earth and Environmental Sciences, University of Wollongong, Australia, following the methods of Norrish and Chappell (1977). Major elements were measured on samples fused with Li borate, whereas trace elements were analysed from pressed pellets bonded with polyvinyl acetate (PVA). Calibration was made against a wide range of international reference materials and laboratory standards previously calibrated against synthetic standards. Loss-on-ignition was determined by heating a
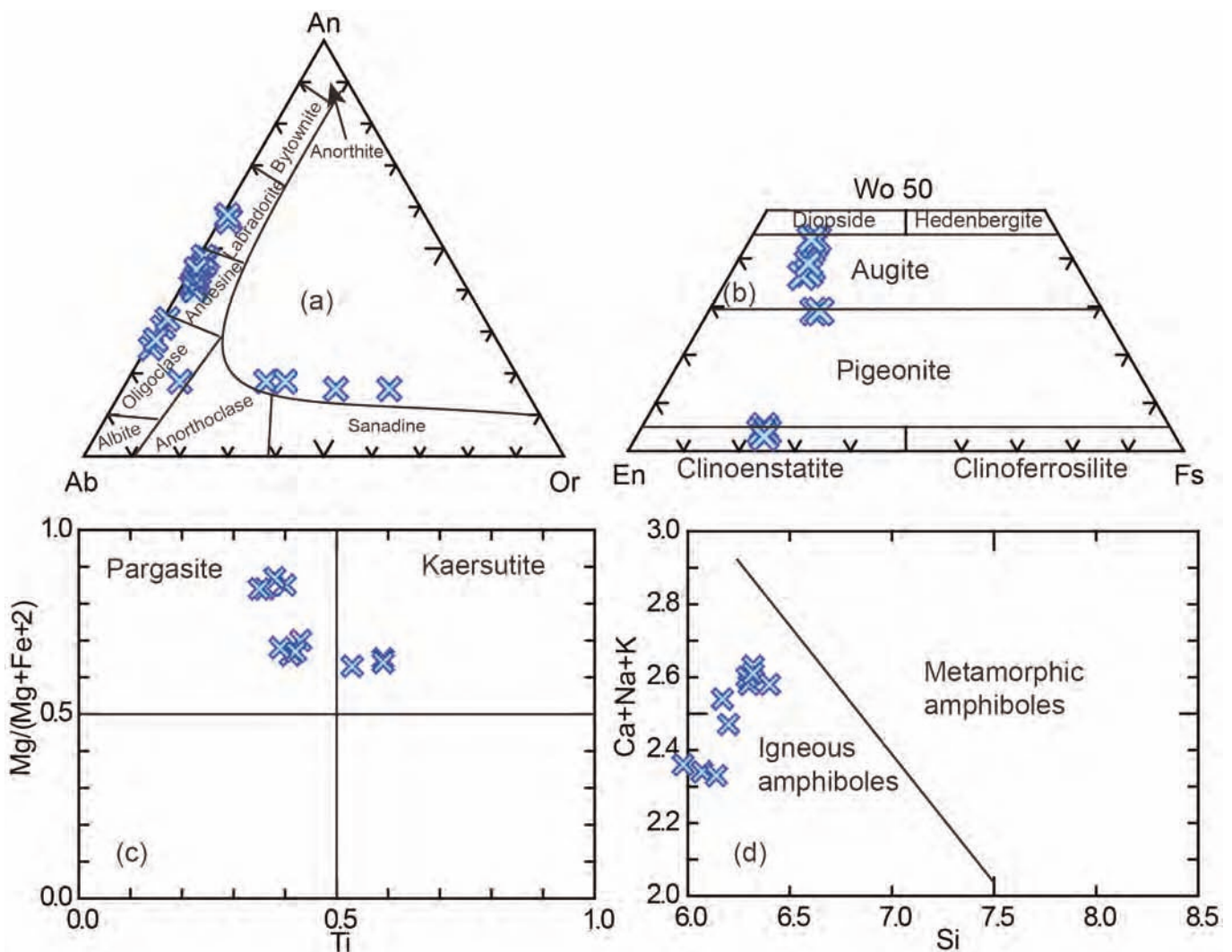

Fig. 5 - (a) Feldspar classification diagram (after Deer et al., 1997); (b) Pyroxene ternary diagram showing clinopyroxene and orthopyroxene compositions from Shaki-Rash gabbro with the nomenclature fields of Morimoto et al., (1988); (c) Composition of amphibole in the Shaki-Rash gabbro rocks (after Leake et al., 1997); and (d) Distinction between igneous and metamorphic amphiboles in the Shaki-Rash gabbro (after Giret et al., 1980).

separate aliquot of rock powder at 1000°C. Examples of recent results on international standards run as unknowns are given in Supplementary Material Tables 8 (majors) and 9 (trace elements). Using inductively coupled plasma-mass spectroscopy (ICP-MS). The samples were analysed at the Australian Laboratory Services (ALS) at Brisbane, Australia, for their rare earth element (REE) and other trace-element concentrations.

PETROGRAPHY AND MINERAL CHEMISTRY

The Shaki-Rash gabbro is fresh and medium- to coarse-grained. Its essential mineral composition includes 50-60% plagioclase, 10-20% olivine, 5-15% clinopyroxene and 5-15% brown hornblende, with lesser (2-6%) orthopyroxene, biotite and alkali feldspar, and minor iron oxides, apatite and zircon. The rocks show dominantly intergranular and poikilitic textures (see Fig. 4a, b).

Plagioclase is mostly andesine to oligoclase (An_{58-26}) and alkali feldspar is Or_{55-11} (Figs 4a-e, 5a plus Fig. S1 and Table S1 in Supplementary Material). The alkali feldspar compositions indicate high temperatures of crystallization while the lack of perthitic texture indicates rapid cooling. Olivine is the most abundant mafic phase, it is included in poikilitic plagioclase and is often rimmed by orthopyroxene in a peritectic relationship (Fig. 4e). The olivine is unusually fresh for Zagros suprasubduction zone assemblages and is rounded to sub-rounded with a composition of Fo_{51-71} (Fig. 4a, b, d, e plus Table S2 in Supplementary Material). The modest Fo_{51-71} content of the olivine, along with its equilibrium textures with other minerals, strongly suggests a magmatic origin for this phase. In fact, xenocrystic from the depleted mantle or xenocrysts formed during the contact metamorphism with dolomitic sedimentary rocks would have been characterized by a much higher forsterite content. Orthopyroxene is usually present as < 0.1 mm rims on olivine or as 0.1-0.3 mm interstitial crystals (Fig. 4e). Orthopyroxene rims of enstatite composition Wo_4 En_{73} Fs_{23}, formed between the plagioclase and olivine, while clinopyroxene is mostly augite Wo_{29-44} En_{44-52} Fs_{11-20} (Figs 4b, e and 5b plus Table S3 in Supplementary Material). Exsolution lamellae of orthopyroxene are absent in the clinopyroxene. Minerals that crystallized from, or by reaction with, intercumulus melt include orthopyroxene (after olivine), amphibole (after clinopyroxene) and biotite. Primary amphibole is mostly kaersutite-pargasite with Mg-values of 0.66-0.87 and with 2.99-4.97 wt% TiO_2 (Figs 4 c, d and 5c, d plus Table S4 in Supplementary Material). Magmatic biotite mostly occurs around the kaersutite (Fig. 4c plus Fig. S2 and Table S5 in Supplementary Material). Fe-Ti oxides comprise 2-6% of the olivine gabbro samples. Ilmenite is the most common oxide and forms irregular interstitial grains or inclusions in olivine and kaersutite. Ti-magnetite occurs along the cleavages and cracks of olivine and/or surrounded by biotite and olivine (see Fig. 4c, d plus Table S6 in Supplementary Material).

Biotite formed late in the crystallization sequence and exhibits a restricted range in composition with 4.10-4.59 wt% TiO_2, 12.19-12.44 wt% FeO, 14.39-14.92 wt% Al_2O_3 and 1.07-1.28 Na_2O. Its high Na_2O and Mg# (0.64-0.65) and textural relationships with kaersutite confirm a magmatic origin. Epidote is observed in some samples (e.g., SR16) associated with albite indicating the effects of minor post-magmatic hydrothermal alteration (see Table S7 and Fig. S1 in Supplementary Material).

RESULTS AND INTERPRETATIONS

SHRIMP U-Pb results

The single zircon fragment shows well-defined oscillatory zoning parallel to the euhedral grain exterior, with local recrystallization of part of the exterior (Fig. 6). Five analyses were undertaken, 4 on the grain interior and 1 on the non-recrystallized part of the exterior (Fig. 6, Table 1). The sites have moderate to high U content (187-835 ppm.) with high Th/U (0.79-1.65). Common Pb abundance is low ($^{204}Pb/^{206}Pb \leq 0.0032$) and prior to correction for common Pb, all analytical sites have close to concordant U-Pb ages, indistinguishable from each other (Fig. 7). Uncorrected for common Pb they yield a weighted mean $^{206}Pb/^{238}U$ age of 39.0±0.5 Ma (95% confidence, MSWD = 0.71) and corrected for common Pb an age of 38.7±0.6 Ma (MSWD = 0.80).

Whole rock geochemistry

The major and trace element (including REE) geochemistry of the investigated 16 olivine gabbro and olivine-amphibole diorite is presented in Table S10 in Supplementary Material. The samples exhibit low loss-on-ignition (LOI) values (-0.01-1.96) excluding three samples (SR6, SR7 and SR8) which are more altered than the others (see Table S10 in Supplementary Material). The textural evidence from thin section petrography, the low LOI and the lack of scatter in mobile LILE elements (Table S10 in Supplementary Material) indicate little chemical disturbance by post magmatic processes.

All analysed rocks, with the exception of one sample SR6 (which is altered), are characterized by low SiO_2 (44.17-51.28 wt%). Al_2O_3 contents range from 14.55-20.30 wt%, CaO ranges from 7.03-12.66 wt% and Na_2O ranges from 2.48-5.81 wt%. The olivine gabbros contain between 5.24-11.57 wt% Fe_2O_3 and 0.42-3.68 wt% TiO_2 with Mg# [Mg# = Mg/(Mg+Fe^{2+})] ranging from 47 to 71. As observed in thin section, the difference in whole-rock chemistry between the analysed samples appears to be mainly controlled by plagioclase + olivine ± clinopyroxene ± orthopyroxene ± amphibole sorting and accumulation. Harker diagrams show the decrease of MgO, Fe_2O_3, Cr and stable to increasing position of CaO, Na_2O and K_2O with increasing SiO_2 for gabbroic rock, which confirms the separation
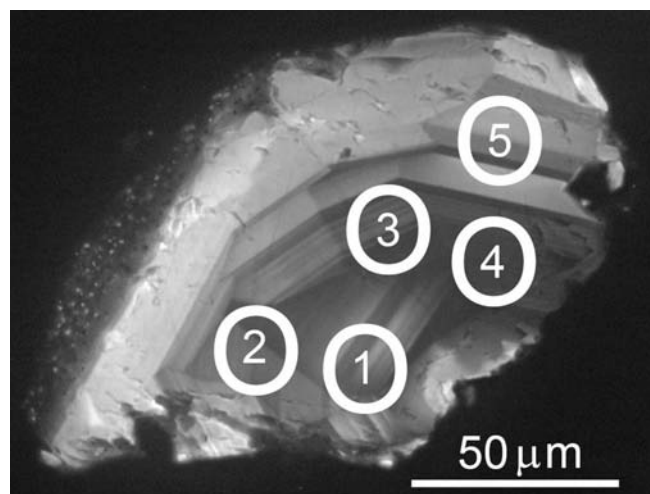

Fig. 6 - Cathodoluminescence (CL) image of the Shaki-Rash gabbro zircon, with the analytical sites indicated.

Table 1 - SHRIMP zircon U-Pb data of Shaki-Rash gabbro samples (SR16, SR26, D2).

Spot	Site	U/ppm	Th/ppm	Th/U	204Pb/206Pb	±	238U/206Pb (meas)	±	207Pb/206Pb (meas)	±	age 206Pb/238U (meas)	±	age 206Pb/238U (corr)	±
1.1	m,osc,p,fr	432	344	0.79	0.0027	0.0012	163.77	2.16	0.049	0.0022	39.24	0.52	37.26	0.98
1.2	m,osc,p,fr	808	1336	1.65	<0.0001	0.0003	166.41	1.77	0.05	0.0022	38.62	0.41	38.62	0.46
1.3	m,osc,p,fr	706	945	1.34	0.0003	0.0002	160.86	4.8	0.0465	0.0024	39.95	1.19	39.72	1.19
1.4	m,osc,p,fr	835	1118	1.34	<0.0001	<0.0001	165.09	1.89	0.0481	0.0017	38.93	0.45	38.93	0.45
1.5	e,osc,p,fr	187	184	0.98	0.0018	0.0032	160.66	3.85	0.0496	0.0038	40	0.95	38.65	2.59

Spot: x.y = grain followed by analysis number
Site: m = middle, e = end, p = prismatic grain, osc = oscillatory zoned, fr = fragment
Isotopic ratios and ages: meas = measured, corr = corrected for common Pb (Cumming and Richards (1975) 40 Ma Pb)
Analytical errors: all are reported at 1ó level

of some Fe-Mg-rich minerals such as olivine and pyroxene during crystallization (Fig. S3 in Supplementary Material). Based on the total alkali content (2.49-6.91 wt%), all samples can be classified as alkaline gabbros according to the schemes of Cox et al., (1979) and De La Roche et al., (1980; Fig. 8a, b). The olivine gabbros are poor in both Ni and Cr, and rich in Sr, in agreement with the higher modal proportions of plagioclase and the low modal proportion of olivine + spinel.

According to the Shervais (1982) Ti-V diagram, most of the olivine gabbro samples have Ti/V from 100 to 50 and consequently fall in the back-arc basin (BAB) and alkaline fields. In contrast, most of the older host intrusions of the Bulfat Igneous Complex (gabbros-granitoids; after Al-Sheraefy, 2009) show a more subduction-related signature (Fig. 9c). This diagram indicates back-arc basin affinity or arc rifting affinities of the olivine gabbro discussed here. The Th/Yb vs Nb/Yb diagram after Pearce (2008) is useful for examining the melt source and contaminants. This is because normalizing both axes to Yb eliminates most effects of partial melting and fractional crystallization (Pearce, 1983). On this diagram, most of the studied rocks fall within the MORB-OIB array, close to the EMORB field. This suggests that they formed in a rifting arc setting (Ishizuka et al., 2002; 2006; Escuder et al., 2008), whereas it is clear that the older intrusive phase of the Bulfat Igneous Complex (Al-sheraefy, 2009) show more arc subduction- related signature (Fig. 8d).

Normalized to chondrite values of Sun and McDonough (1989), the REE patterns of the olivine gabbros are LREE enriched (Ce_N/Yb_N = 1.09-7.0) and parallel, with the HREE about 9 times chondrite (Fig. 8e). The presence of a positive Eu anomaly (Eu/Eu* = 0.71-2.85) suggest accumulation of plagioclase (Fig. 8e). In multi-element spider plots normalized to primitive mantle of Sun and McDonough (1989), the olivine gabbros show that LREE and other highly incompatible trace elements are enriched, whereas Y and the HREE are depleted. Nb-Ta-Zr-anomalies that would indicate subduction-related magmatism and/or significant crustal contamination are absent from the trace element patterns (Fig. 8f).
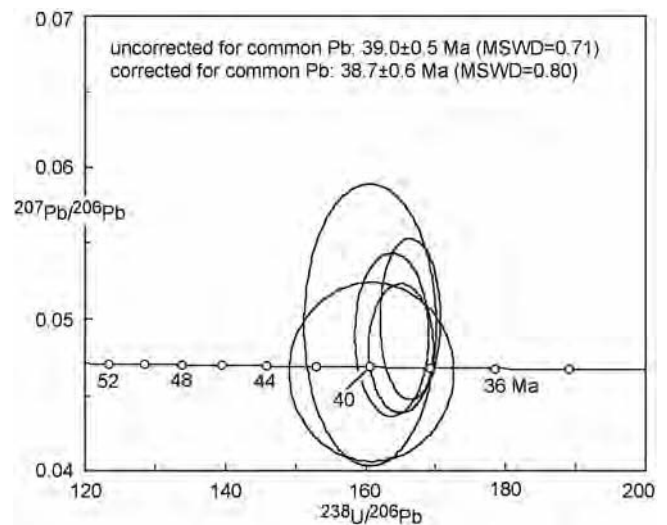

Fig. 7 - $^{238}U/^{206}Pb$ – $^{207}Pb/^{206}Pb$ plot, uncorrected for common Pb. Analytical errors are depicted at the 2 sigma level.
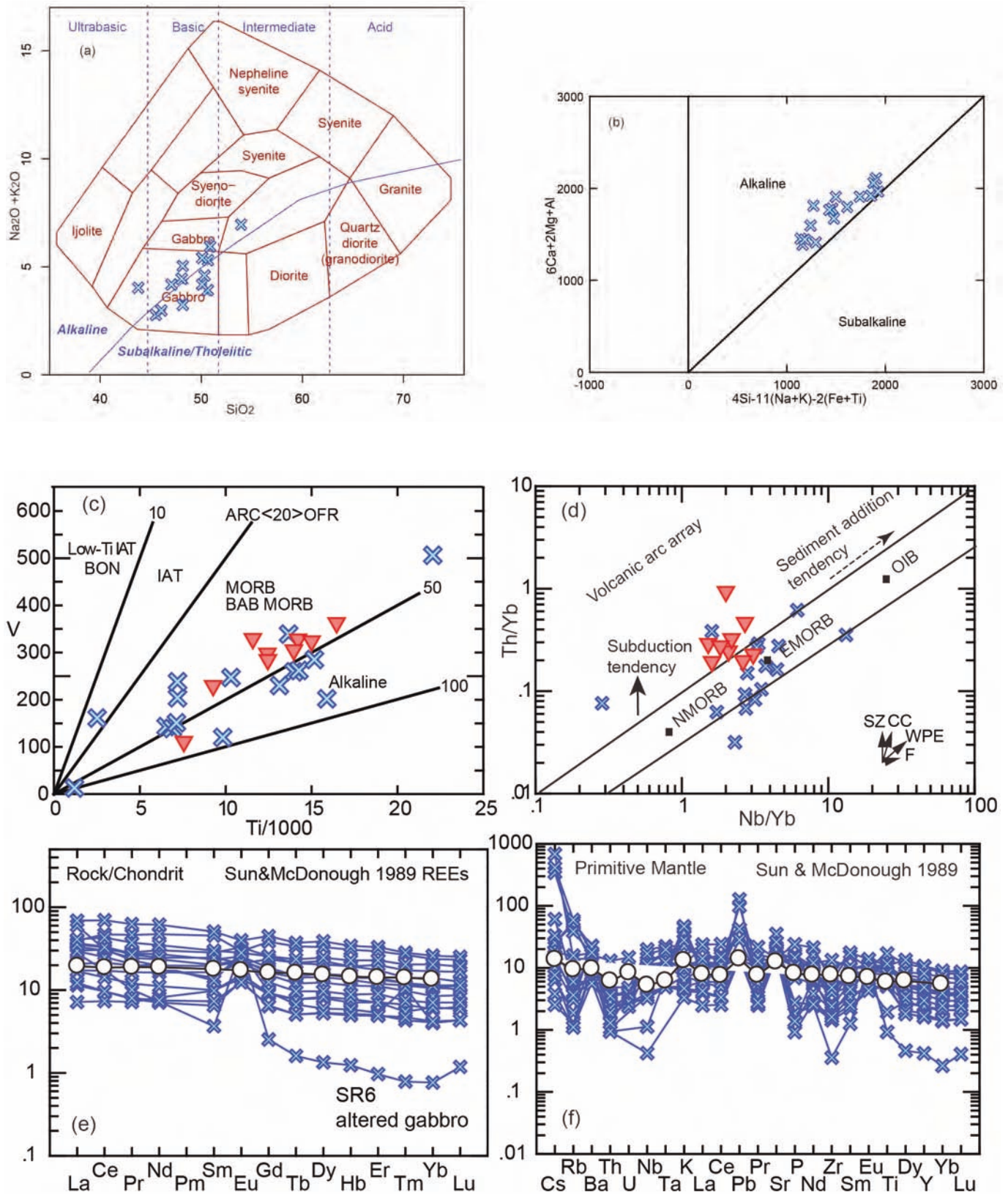
Fig. 8 - Variation diagrams for Shaki-Rash gabbro. (a) Classification of the gabbroic rocks using the diagram of Cox et al., (1979). (b) Multicationic classification plot of De La Roche et al., (1980; R1 = 4Si - 11(Na + K) - 2(Fe + Ti); R2 = 6Ca + 2Mg + Al). (c) Tectonic discrimination diagram between V and Ti/1000 (after Shervais, 1982), red triangle samples are host rock arc-related samples from Al-Sheraefy (2009). (d) Th/Yb vs Nb/Yb (after Pearce, 2008) showing most of the Bulfat olivine gabbro rocks plot within the MORB array. OIB- oceanic island basalt; SZ- subduction zone enrichment; CC- crustal contamination; F- fractional crystallization; WPE- within plate enrichment; N-MORB- normal mid-ocean-ridge basalt; E-MORB- enriched mid-ocean-ridge basalt. (e) Chondrite normalized plots for the Shaki-Rash gabbro rocks. (f) Primitive mantle normalized plots for Shaki-Rash gabbro rocks; both chondrite and primitive mantle values are from Sun and McDonough (1989). The red circle represents the average for Central Mariana Trough lavas (CMT12-8; after Pearce et al., 2005).

DISCUSSION

Amphibole geothermobarometry

The freshness of the mineral assemblages in the Shaki-Rash gabbro in the Bulfat Igneous Complex Composition of igneous Ca-amphibole can provide constraints on the crystallization history of magmas. This is because Ti occupancy in amphibole depends strongly on temperature (T) (Schmidt, 1992; Anderson and Smith, 1995; Ernst and Liu, 1998), whereas isopleths for Al_2O_3 in Ca-amphibole exhibit markedly negative P-T slopes, indicating increasing Al_2O_3 contents with both P and T. In contrast, TiO_2 isopleths are strongly temperature dependent and nearly independent of P. Ernst and Liu (1998) compiled a pressure-temperature (P-T) scheme based on the Al_2O_3 and TiO_2 contents in amphiboles. Using this scheme, the Bulfat olivine gabbro kaersutites can be classified as a high-temperature magmatic phase, probably crystallized between 950-1050ºC (i.e., Ti vs. Al; Fig. 9a, b) and the pressures of crystallization for the investigated amphibole is between 5 and 3 kbar (Ernst and Liu, 1998; Fig. 9b).

Interpretation of the ~ 40 Ma zircon age

Given the gabbroic nature of the rock, a very low yield of zircons was expected from a sample of less than 200 g in weight. However, as only one zircon was retrieved, it should be examined whether this grain was truly derived from the Shaki-Rash gabbro or if it could be a laboratory contaminant. The Shaki-Rash gabbro sample was processed through the laboratory at the same time as a batch of samples that are Jurassic and older in age, which have zircons ranging in age from 120 Ma back to Archaean. This reduces the possibility of cross contamination, because any expected contaminant grains should be 120 Ma or older. Thus I have confidence that the single Cenozoic zircon recovered was indeed sourced from the Shaki-Rash sample, and is not a laboratory contaminant. Support for this conclusion comes from the analysed zircon having the same age within error as zircons recovered from other arc allochthons in Kurdistan - an unlikely scenario if this grain is a random laboratory contaminant.

The low yield of zircon from the gabbro is typical. Until the last stages of gabbro magma crystallization, zirconium is incorporated into clinopyroxene. It is only in the last randomly-distributed pockets of residual melt, that the melt becomes silica oversaturated and zircons start to crystallize. Therefore I am confident that the grain (i) truly comes from the Shaki-Rash gabbro and (ii) it is magmatic in origin. Furthermore, I note the high Th/U of the zircon (0.79-165), in range typical of zircons grown out of a gabbroic melt, rather than more siliceous tonalitic-granitic melts (which have lower Th/U of typically 0.2-0.6).

With the authenticity of the grain established, the question then needs to be asked, how accurate is the age (~39 Ma - Eocene, Bartonian)? In order to have certainty over this, the Temora grains used for data calibration were distributed in several different clusters across the mount. During the course of analysis, these were visited randomly, and display no significant bias in their apparent ages. This means that the calibration is reliable, and has not been compromised by mount preparation (or instrumentation issues). In due consideration of these factors, we interpret ~ 39 Ma as an accurate determination of the crystallization age for the Shaki-Rash gabbro.

Geodynamic setting of the Shaki-Rash gabbro in Neotethys

The integrated field, mineralogical and whole rock geochemical evidence indicate that the Shaki-Rash olivine gabbros are alkaline in character and were intruded into an assemblage of intra-oceanic suprasubduction rocks. These dykes do not continue into other allochthonous thrust sheets. Therefore, they are not a result of late orogenic tectonic collapse, after assemblage of intra-oceanic allochthons on the Arabian margin. Instead, the Shaki-Rash gabbro is restricted to one intra-oceanic allochthon, and is interpreted to indicate arc rifting. Geochemical evidence for this is that the host Cenozoic plutonic rocks of the Shaki-Rash gabbro show clear suprasubduction related geochemical signatures, such as elevated Th/Nb relative to Nb/Yb, placing these in the arc field, whereas the Shaki-Rash olivine gabbros fall in the MORB-EMORB-array (Fig. 8d). Mild enrichment of the LREE relative to HREE, without discernable negative Nb, Ta, Ti anomalies but with enrichment in K, Pb, Rb and Cs, is another signature suggesting an enriched mantle source with a diminished or minimal subduction-related component. This signature is similar to that documented for mafic rocks formed in modern arc-rifting (e.g., Mariana Trough; Taylor et al., 1996; Pearce et al., 2005; Fig. 8e, f).
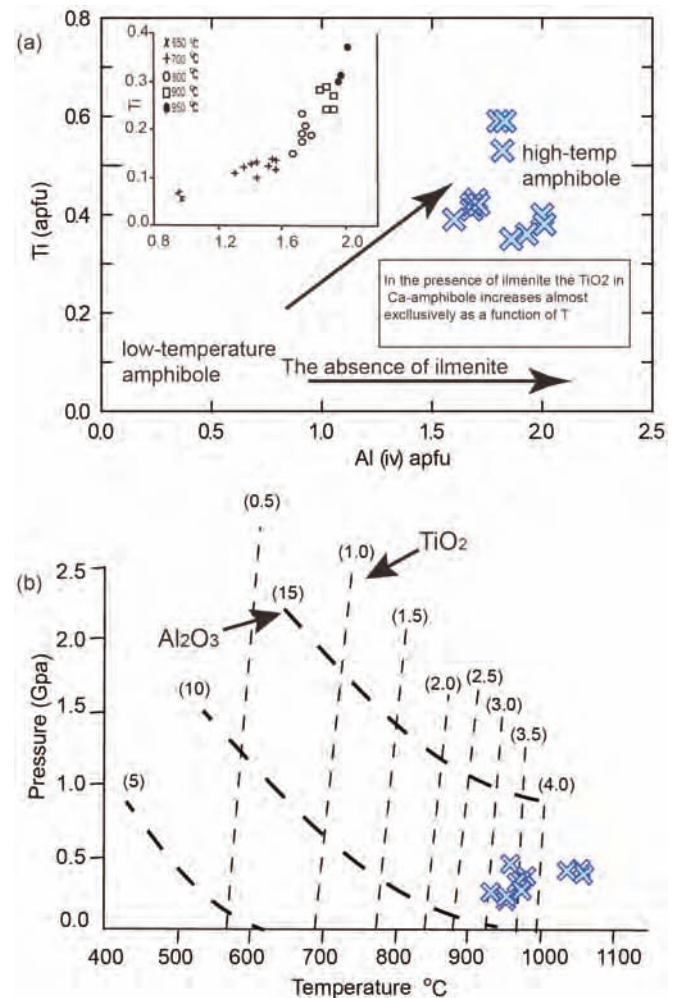

Fig. 9 - (a) Correlation of Al^{iv} and Ti contents of amphibole in the Shaki-Rash gabbro (after Ernst and Liu, 1998). (b) Isopleths of Al_2O_3 and TiO_2 in weight percent of the amphiboles show that they formed at between 950-1050ºC and < 5 kbar, equivalent to depths of 8-15 km (after Ernst and Liu, 1998).

This first recognition of arc rifting in the Iraqi Cenozoic intra-oceanic suprasubduction assemblage adds another dimension of complexity of the late stage processes shortly before closure of Neotethys. This new information is added to an increasingly high resolution reconstruction of ocean closure of Neotethys in Iraq that has resulted from a programme of integrated geochemical and modern geochronological studies (Aswad et al., 2011; 2013; 2016; Ali et al., 2016).

Geodynamic reconstruction

The age and relationships between the successive nappes in the Zagros Suture Zone is still somewhat contentious. Earlier research described the igneous activity in the Bulfat Igneous Complex (Buda, 1993; Jassim et al., 2006) and indicated a possible linkage between this igneous activity and the Walash-Naopurdan successions preserved in the Lower Allochthon. Subsequent geochemical analyses of the Bulfat suite have clearly indicated that these igneous assemblages are not related and that they formed in separate subduction zone systems (Aswad et al., 2013; 2016). Until recently, the age of the Bulfat Igneous Complex had not been clearly defined, and was thought to have been emplaced at about 45 Ma (Paleocene; Aswad et al., 2013). Subsequent $^{40}Ar/^{39}Ar$ age determinations on hornblende and biotite have established a Paleocene age (39.2±0.2 Ma and 38.9±0.2 Ma) for the main intrusions in the complex (Aswad et al., 2016). The 39 Ma zircon age (this study) has established a reliable age of the Shaki-Rash gabbro represents one of the younger intrusions within the Bulfat Igneous Complex.

There is debate as to the timing, duration, number and the geographic distribution of the subduction systems that closed Neotethys. The zircon geochronological U-Pb result presented here indicates that at ~ 39 Ma, arc rifting occurred in an intra-oceanic suprasubduction assemblage. Based on this new knowledge I propose here a synthesis for the subduction systems that closed the Neotethys Ocean along the Iraqi sector of the Zagros Suture Zone (Fig. 10).

A first key finding for this sector is that subduction was active in the Cretaceous (Azizi and Jahangiri, 2008; Aswad et al., 2016). It was not, as proposed by Alvarez (2010), a 'quiet zone' between active subduction to the south in Iran-Oman and to the north in Turkey-Eastern Mediterranean. During the Early Cretaceous, subduction of part of the Neotethyan oceanic crust towards east and northeast developed an ophiolite complex represented in Iraq by the Penjween, Mawat, Pushtashan and Hasanbag bodies (Fig. 10a). This was distal from Eurasia, which lay at the northeastern margin of the Neotethys Ocean. Collision of the Cretaceous ophiolite complexes onto the Arabian passive margin occurred during the Late Cretaceous. This coincided with obduction of other ophiolites, including the Kermanshah-Penjween ophiolites, over the northeastern margin of the Arabian Plate (Jassim and Goff, 2006; Azizi and Moinevaziri, 2009; Shafaii and Stern, 2011; Agard et al., 2011; Ali et al., 2012; Fig. 10b).

Secondly, as argued on the lines of evidence presented by Aswad et al. (2016), there were two coeval Eocene subduction systems. This model is summarized as cartoon cross-sections in Fig. 10, and draws not only on information presented in this paper, but also on the results in recent papers (Ali et al., 2012; Aswad et al., 2013; 2016). The mechanism by which the short-lived Paleogene dual subduction zone system was initiated is not clear yet. However, recent research by Agard et al. (2005; 2007; 2011) and Alzerez (2010) proposed that an acceleration of the convergence rate would have increased the resistance of the asthenospheric mantle to the subducting Neotethyan slab and transmitted compressional
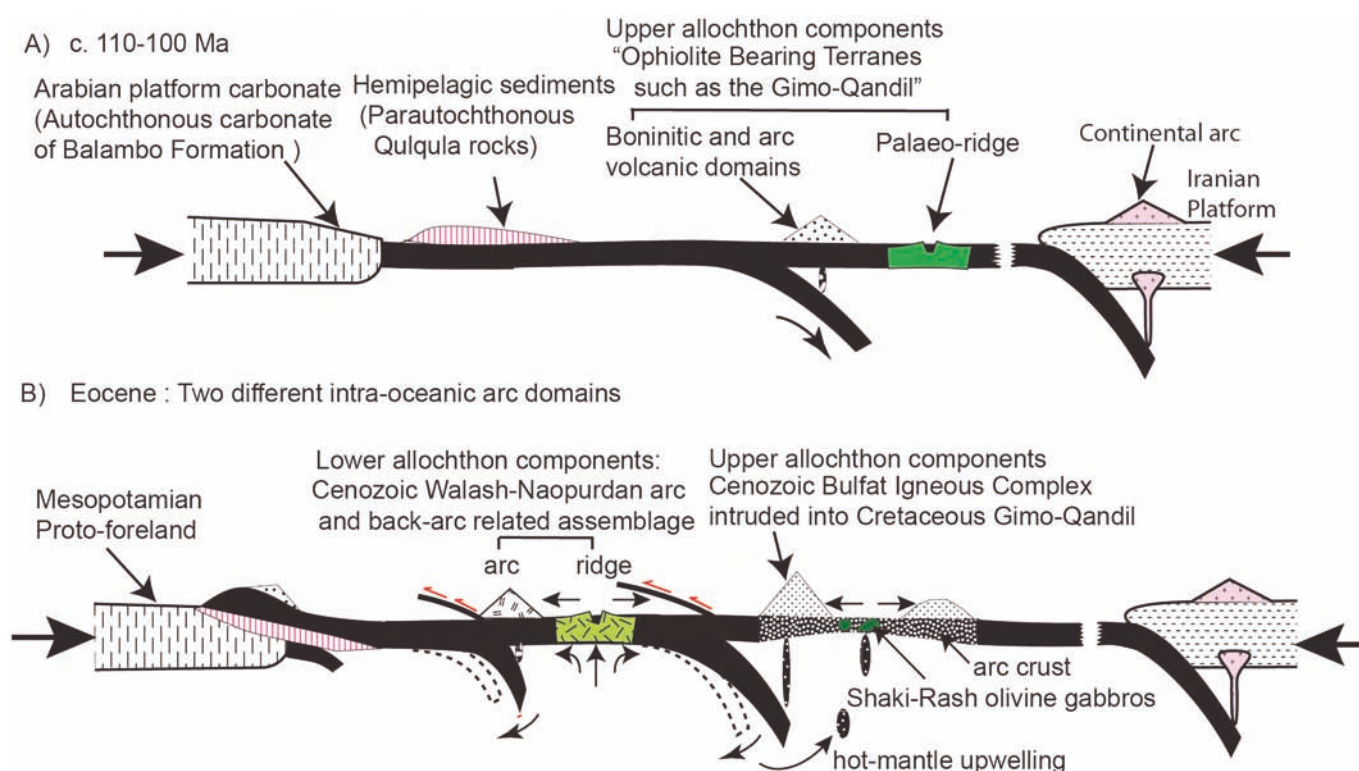

Fig. 10 - Schematic diagram presenting the tectonic evolution model of the Shaki-Rash gabbro within a Neotethys Cenozoic arc.

stresses across the plate near the Arabian Platform. The resistance, however, would have caused stresses to accumulate in the oceanic lithosphere leading to the termination of the Cretaceous-Middle Eocene arc magmatism phase.

An island-arc complex developed in the Neotethys to eventually form the Eocene-Oligocene Walash-Naopurdan Groups, when it the initiation of a short-lived additional subduction zone of Paleogene age within the oceanic crust near the Arabian Platform culminated with arc volcanic activity expressed by the Walash-Naopurdan Middle Eocene to Oligocene suprasubduction zone assemblage (Aswad et al., 2016) that was subsequently accreted to the Arabian margin.

The third finding was that the Bulfat Igneous Complex represents an additional short-lived subduction zone superimposed Eocene arc magmatism into the Cretaceous suprasubduction complex, indicating long-lived or reactivated arc magmatism in the oceanic realm. Later rifting, due to rollback, led to ablation of the lithosphere and mantle upwelling to produce the melt that gave rise to the Shaki-Rash gabbro.

CONCLUSIONS

(1) The Shaki-Rash gabbros are late intrusions into the arc-related Bulfat Igneous Complex in the Upper Allochthon of the Zagros collision zone (northeast of Hero town, NE Iraq).

(2) The Shaki-Rash gabbro has an alkaline character and amphibole chemistry that indicates it crystallized at ~ 5-3 kbar and ~ 950-1050°C.

(3) A zircon U-Pb age of 39 Ma is an accurate determination of the Shaki-Rash gabbro crystallization age.

(4) The major, trace and REE geochemistry and field relations indicate that the olivine gabbro rocks formed in the suprasubduction zone within an arc rifting setting. As such this is the first evidence of arc rifting in Iraqi suprasubduction zone assemblages.

ACKNOWLEDGEMENTS

REFERENCES

Agard P., Jolivet L., Vrielynck B., Burov E. and Monié P., 2007. Plate acceleration: the obduction trigger? Earth Planet. Sci. Lett., 258: 428-441.

Agard P., Omrani J., Jolivet J. and Mouthereau F., 2005. Convergence history across Zagros (Iran): constraints from collisional and earlier deformation. Intern. J. Earth Sci.., 94: 401-419.

Agard P., Omrani J., Jolivet L., Whitechurch H., Vrielynck B., Spakman W., Monie P., Meyer B. and Wortel R., 2011. Zagros orogeny: a subduction-dominated process. Geol. Mag., 148: 692-725.

Ali S.A., Buckman S., Aswad K.J., Jones B.G., Ismail S.A. and Nutman A.P., 2012. Recognition of Late Cretaceous Hasanbag ophiolite-arc rocks in the Kurdistan region of the Iraqi Zagros Thrust Zone: A missing link in the paleogeography of the closing Neo-Tethys Ocean. Lithosphere., 4: 395-410, doi: 10.1130/L207.1.

Ali S.A., Buckman S., Aswad K.J., Jones B.G., Ismail S.A. and Nutman A.P., 2013. The tectonic evolution of a Neo-Tethyan (Eocene-Oligocene) island-arc (Walash-Naopurdan Group) in the Kurdistan region of the NE Iraqi Zagros Thrust Zone. Isl. Arc., 22: 104-125, doi: org/10.1111/iar.12007.

Ali S.A., Ismail S.A., Nutman A.P., Bennett V.C., Jones B.G. and Buckman S., 2016. The intra-oceanic Cretaceous (~ 108 Ma) Kata-Rash arc fragment in the Kurdistan segment of Iraqi Zagros suture zone: Implications for Neotethys evolution and closure. Lithos., 260: 154-163.

Al-sheraefy R. M., 2009. Petrographic, geochemical and tectonic evidence of granitoid - gabbro, Bulfat Complex, Qala Deza / North-East Iraq (M.Sci. thesis): Univ. Mosul, College Sci., Iraq (in Arabic), 179 pp.

Alvarez W., 2010. Protracted continental collisions argue for continental plates driven by basal traction. Earth Planet. Sci. Lett., 296: 434-442.

Anderson J.L. and Smith D.R., 1995. The effects of temperature and fO_2 on the Al in hornblende barometer. Am. Miner., 80: 549-559.

Aswad K.J., Al-sheraefy R.M. and Ali S.A., 2013. Pre-collisional intrusive magmatism in the Bulfat Complex, Wadi Rashid, Qala Deza, NE Iraq: Geochemical and mineralogical constraints and implications for tectonic evolution of granitoid-gabbro suites. Iraqi Nat. J. Earth Sci., 13: 103-137.

Aswad K.J., Ali S.A., Al-sheraefy R.M., Nutman A.P., Jones B.G., Buckman S. and Jourdand F., 2016. $^{40}Ar/^{39}Ar$ hornblende and biotite geochronology of the Bulfat Igneous Complex, Zagros Suture Zone, NE Iraq: New insights on complexities of Paleogene arc magmatism during closure of the Neotethys Ocean. Lithos., 266-267: 406-413.

Aswad K.J., Aziz N.R. and Koyi H.A., 2011. Cr-spinel compositions in serpentinites and their implications for the petrotectonic history of the Zagros Suture Zone, Kurdistan Region, Iraq. Geol. Mag., 148: 802-818.

Aziz N.R., Aswad K.J and Koyi H.A., 2011. Contrasting settings of serpentinite bodies in the northwestern Zagros Suture Zone, Kurdistan Region, Iraq. Geol. Mag., 148: 819-837, doi: 10.1017/S0016756811000409.

Azizi H. and Jahangiri A., 2008. Cretaceous subduction-related volcanism in the northern Sanandaj-Sirjan Zone, Iran. J. Geodyn., 45: 178-190.

Azizi H. and Moinevaziri H., 2009. Review of the tectonic setting of Cretaceous to Quaternary volcanism in northwestern Iran. J. Geodyn., 47:167-179.

Black L.P., Kamo S.L., Allen C.M., Aleinikoff J.M., Davis D.W., Korsch R.J and Foudoulis C., 2003. TEMORA 1: a new zircon standard for Phanerozoic U-Pb geochronology. Chem. Geol., 200: 155-170.

Buda GY., 1993. Igneous petrology of the Bulfat Area (North-East Iraqi Zagros Thrust Zone). Acta Miner. Petrogr., Szeged, 34: 21-39.

Cox K.G., Bell J.D. and Pankhurst R.J., 1979. The interpretation of igneous rocks. Chapman and Hall, London, 450 pp.

Cumming G.L. and Richards J.R., 1975. Ore lead ratios in a continuously changing Earth. Earth Planet. Sci. Lett., 28: 155-171.

Deer W.A., Howie R.A. and Zussman J., 1997. Rock-forming minerals. Geol. Soc. London, 4, 973 pp.

De La Roche H., Leterrier J., Grandclaude P. and Marchal M., 1980. A classification of volcanic and plutonic rocks using R1-R2 diagrams and major element analyses. Its relationship and current nomenclature. Chem. Geol., 29: 193-210.

Ernst W. G and Liu J., 1998. Experimental phase-equilibrium study of Al- and Ti-contents of calcic amphibole in MORB L. A. Semiquantitative Thermobarometer. Am. Miner., 83: 952-969.

Escuder J., Joubert M., Urien P., Friedman R., Weis D., Ullrich T. and Pérez-Estaún T., 2008. Caribbean island-arc rifting and back-arc basin development in the Late Cretaceous: Geochemical, isotopic and geochronological evidence from Central Hispaniola. Lithos., 104: 378-404.

Gill J. and Whelan P., 1989. Early rifting of an oceanic island arc (Fiji) produced shoshonitic to tholeiitic basalts. Geophys. Res., 94: 4561-4578.

Giret A., Bonin B. and Leger J.M., 1980. Amphibole compositional trends in oversaturated and undersaturated, alkaline plutonic ring complexes. Can. Miner., 18: 481-495.

Hawkins J.W., Bloomer S.H., Evans C.A. and Melchior J.T., 1984. Evolution of intra-oceanic arc-trench systems. Tectonophysics., 102: 174-205.

Ishizuka O., Kimura J.I., Li Y.B., Stern R.J., Reagan M.K., Taylor R.N., Ohara Y., Bloomer S.H., Ishii T., Hargrove U.S. and Haraguchi S., 2006. Early stages in the evolution of Izu-Bonin arc volcanism: new age, chemical, and isotopic constraints. Earth Planet. Sci. Lett., 250: 385-401.

Ishizuka O., Uto K., Yuasa M. and Hochstaedter A.G., 2002. Volcanism in the earliest stage of back-arc rifting in the Izu-Bonin arc revealed by laser-heating $^{40}Ar/^{39}Ar$ dating. J. Volcan. Geoth. Res., 120: 71-85.

Jassim S.Z. and Goff J.C., 2006. Geology of Iraq., Dolin, Prague and Moravian Museum, Brno, 341 pp.

Jassim S.Z., Suk M. and Waldhausrova J., 2006. Magmatism and metamorphism in the Zagros Suture. In: S.Z. Jassim and J.C Goff (Eds), Geology of Iraq. Dolin, Prague and Moravian Museum, Brno, p. 212-231.

Jassim S.Z.,Waldhausrova J. and Suk M., 1982. Evolution of magmatic activity in Iraqi Zagros complexes. Krystalinikum, 16: 87-108.

Kimura J.I. and Stern R.J., 2008. Neogene volcanism of the Japan Island Arc: the K-h relationship revisited. Circum-Pacific tectonics, geologic evolution, and ore deposits Symp. Arizona Geol. Soc. Digest. Proceed. Vol., p. 187-202.

Kretz R., 1983. Symbols for rock-forming minerals. Am. Miner., 68: 277-279.

Larter R.D. and Leat P.T., 2003. Intra-oceanic subduction systems: Tectonic and magmatic processes. Geol. Soc. London Spec. Publ., 219: 1-17.

Leake B.E., Woolley A.R., Arps C.E.S., Birch W.D., Gilbert M.C., Grice J.D., Hawthorne F.C., Kato A., Kisch H.J., Krivovichev V.G., Linthout K., Laird J., Mandarino J.A., Maresch W.V., Nickel E.H., Rock N.M.S., Schumacher J.C., Smith D.C., Stephenson N.C.N., Ungaretti L., Whittaker E.J.W. and Youzhi G., 1997. Nomenclature of amphiboles: report of the Subcommittee on Amphiboles of the Intern. Miner. Ass., Commission on New Minerals and Mineral Names. Am. Miner., 82: 1019-1103.

Ludwig K.R., 2003. Isoplot 3.0: a geochronological toolkit for Microsoft Excel. Berkeley Geochronological Center Spec. Publ., 4, 70 pp.

Morimoto N., Fabries J., Ferguson A.K., Ginzburg I.V., Ross M., Seifert F.A., Zussman J., Aoki K. and Gottardi G., 1988. Nomenclature of Pyroxenes. Miner. Mag., 52: 535-550.

Norrish K. and Chappell B., 1977. X-Ray Fluorescence Spectrometry. Physical methods in determinative mineralogy. Academic Press, London, p. 201-72.

Pearce J.A., 1983. Role of the sub-continental lithosphere in magma genesis at active continental margins. In: C.J. Hawkesworth and M.J. Norry (Eds.), Continental basalts and mantle xenoliths. Shiva Publ. Ltd., Cambridge, p. 230-249.

Pearce J.A., 2008. Geochemical fingerprinting of oceanic basalts with applications to ophiolite classification and the search for Archean oceanic crust. Lithos., 100: 14-48.

Pearce J.A., Stern R.J., Bloomer S.H and Fryer P., 2005. Geochemical mapping of the Mariana arc-basin system: Implications for the nature and distribution of subduction components. Geochem. Geophys. Geosyst., 6: 1-27.

Schmidt M.W., 1992. Amphibole composition in tonalite as a function of pressure: An experimental calibration of the Al-in-hornblende barometer. Contrib. Miner. Petr., 110: 304-310.

Shafaii Moghadam H. and Stern, J.R., 2011. Geodynamic evolution of Upper Cretaceous Zagros ophiolites: formation of oceanic lithosphere above a nascent subduction zone. Geol. Mag., 148: 762-801.

Shervais J.W., 1982. Ti-V plots and the petrogenesis of modern and ophiolitic lavas: Earth Planet. Sci. Lett., 59: 101-118, doi: 10.1016/0012-821X(82)90120-0.

Sun S.S. and Mcdonough W., 1989. Chemical and isotopic systematics of oceanic basalts: Implications for mantle composition and processes. In: A.D. Saunders and M.J. Norry (Eds.), Magmatism in the ocean basins. Geol. Soc. London Spec. Publ., 42: 313-345.

Taylor B. and Karner G.D., 1983. On the evolution of marginal basins, Rev. Geophys., 21: 1727-1741.

Taylor B., Zellmer K., Martinez F. and Goodliffe A., 1996. Seafloor spreading in the Lau backarc basin. Earth Planet. Sci. Lett., 144: 35-40.

Williams S., 1998. U-Th-Pb geochronology by ion microprobe. Rev. Econ. Geol., 7: 1-35.